RSC Advances

PAPER

View Article Online
View Journal | View Issue

Check for updates

Cite this: *RSC Adv.*, 2024, **14**, 2391

Green synthesis of ethyl cinnamates under microwave irradiation: photophysical properties, cytotoxicity, and cell bioimaging†

Miguel Angel Aztatzi-Mendoza,[a] Edgar Leonel Porras-Núñez,[a] Verónica M. Rivas-Galindo,[b] Pilar Carranza-Rosales,[c] Irma Edith Carranza-Torres,[c] Catalina García-Vielma,[c] Iran F. Hernández Ahuactzi,[d] Susana López-Cortina,[a] Israel López *[e] and Eugenio Hernández-Fernández *[a]

A simple and green method for the synthesis of six ethyl cinnamates was performed *via* Horner–Wadsworth–Emmons reaction under microwave irradiation. The photoluminescent properties of all compounds in ethyl acetate solutions were evaluated demonstrating that all compounds exhibit fluorescence. Five compounds exhibited blue emissions in the 369–442 nm range, and another compound exhibited blue-green emission at 504 nm. This last compound showed the largest Stokes shift (134 nm), and the highest quantum yield (17.8%). Two compounds showed extinction coefficient values (ε) higher than 30 000 M^{-1} cm^{-1}, which are appropriate for cell bioimaging applications. In this sense, cytotoxicity assays were performed using Vero cells at different concentrations; the results showed that these compounds were not cytotoxic at the highest concentration tested (20 μg mL^{-1}). Finally, the analysis by fluorescence microscopy for localization and cellular staining using Vero cells demonstrated that the compounds stained the cytoplasm and the nuclei in a selective way.

Received 22nd September 2023
Accepted 22nd December 2023

DOI: 10.1039/d3ra06443c

rsc.li/rsc-advances

Open Access Article. Published on 11 January 2024. Downloaded on 11/12/2024 6:21:54 AM.
This article is licensed under a Creative Commons Attribution-NonCommercial 3.0 Unported Licence.

1. Introduction

The luminescent organic compounds with a π-conjugated system between electron donor (D) and acceptor (A) groups have attracted interest because of their easy purification,[1] high solubility in organic solvents,[2] high quantum efficiency,[3] high molecular and thermal stability,[4] and availability of greener synthetic routes to obtain them. These properties allow their application in organic light-emitting diodes,[5] medicinal chemistry,[6] fluorescence imaging,[7] organic field-effect transistors,[8] organic solar cells,[9] polymer science,[10] forensic science,[11] and chemical sensors.[12]

The application of a fluorescent compound will depend on its properties such as solubility in organic solvents, lipophilicity, chemical reactivity, and photophysical properties namely absorption (λ_{abs}) and emission (λ_{abs}) wavelengths, extinction coefficient (ε), quantum yield (Φ), large achievable Stokes shift, remarkable resistance to photobleaching, lifetime of the excited state, and photostability. Therefore, when these properties reach adequate values in fluorescent organic compounds and proteins, the latter can be used in specific applications such as single molecule tracking, and multicolor bioimaging.[13–21] Fluorescence bioimaging has been of great importance in biomedical, biological, and related sciences because of its essential contributions to understanding life sciences. It is a non-invasive technique that possesses high resolution and allows different intracellular processes to be observed in real time. In recent decades, fluorescent organic compounds have been designed and synthetized with diverse applications including molecular dyes,[22] fluorescent proteins,[23] and luminescent polymers,[24,25] among others. Predominantly, long-term tracking of cells is a great tool in the investigation of biological processes, pathological pathways, and long-term drug therapeutic effects.[26,27] Nowadays, the synthesis of high performance deep-blue fluorophores is of great interest.[28] These blue emitters must exhibit a remarkable efficiency, color purity and stability.[29] The extensive research on deep-blue compounds

[a]*Universidad Autónoma de Nuevo León, UANL, Facultad de Ciencias Químicas, Pedro de Alba s/n, Ciudad Universitaria, 66450 San Nicolás de los Garza, Nuevo León, Mexico. E-mail: eugenio.hernandezfr@uanl.edu.mx; Fax: +52-81-83294000; Tel: +52-81-83294000 ext. 6293*

[b]*Universidad Autónoma de Nuevo León, UANL, Facultad de Medicina, Fco. I. Madero s/n, Mitras Centro, 64460 Monterrey, Nuevo León, Mexico*

[c]*Centro de Investigación Biomédica del Noreste, Instituto Mexicano del Seguro Social, Monterrey 64720, Nuevo León, Mexico*

[d]*Centro Universitario de Tonalá, Universidad de Guadalajara, Av. Nuevo Periférico 555, Ejido San José Tatepozco, Tonalá 45425, Jalisco, Mexico*

[e]*Universidad Autónoma de Nuevo León (UANL), Facultad de Ciencias Químicas, Centro de Investigación en Biotecnología y Nanotecnología, Laboratorio de Nanociencias y Nanotecnología, Autopista al Aeropuerto Internacional Mariano Escobedo Km. 10, Parque de Investigación e Innovación Tecnológica, 66629 Apodaca, Nuevo León, Mexico. E-mail: israel.lopezhr@uanl.edu.mx; Fax: +52-81-83294000; Tel: +52-81-83294000 ext. 4202*

† Electronic supplementary information (ESI) available. See DOI: https://doi.org/10.1039/d3ra06443c

© 2024 The Author(s). Published by the Royal Society of Chemistry

Open Access Article. Published on 11 January 2024. Downloaded on 11/12/2024 6:21:54 AM. This article is licensed under a Creative Commons Attribution-NonCommercial 3.0 Unported Licence.

is currently focused on increasing the efficiency and lifetime of the devices, because these features are lower than those of red and green devices, reaffirming the interest in obtaining high performance deep-blue molecules.[30] The electron donating and withdrawing groups in the emitter structure help to improve their performance.[31] In some cases, the deep-blue fluorophores exhibit multifunctional properties,[32] such as an efficient reduction of energy consumption,[33] an increase in color gamut and the ability of being the host of other large-wavelength fluorophores.[34]

Previous reports have shown that the synthesis of α,β-unsaturated esters can be achieved through conventional synthesis including Wittig and Horner–Wadsworth–Emmons (HWE) reactions, however they involved prolonged reaction times.[35–41] In this paper, we present the synthesis of α,β-unsaturated esters *via* the HWE reaction assisted by microwave irradiation, due to the advantages that this method present, using the appropriate aromatic aldehydes with triethyl phosphonoacetate. The photophysical properties of the fluorescent compounds were studied and the emitters that showed the best performance were tested in cell bioimaging.

2. Experimental section

2.1 Material and equipment

All chemicals and solvents were purchased from commercial sources, and they were used as received. An Electrothermal Mel-Temp apparatus was used to determine the melting points. Thin-layer chromatography was used to follow the progress of the reactions. Column chromatography was used to purify the products using silica gel as the stationary phase. The ^{1}H and ^{13}C NMR spectra were obtained using chloroform-*d* ($CDCl_3$) with tetramethylsilane (TMS) as the solvent and the internal reference, respectively. The NMR spectra were acquired on a Bruker Avance III HD 400 MHz NMR spectrometer (ESI†). Chemical shifts (δ) are reported in ppm and the coupling constants (J) are reported in Hertz (Hz). Multiplicities are reported as: singlet (s), doublet (d), triplet (t), quartet (q), multiplet (m). Mass spectral data were obtained using ESI$^+$ techniques (MStation). A Microwave Synthesis Reactor (Monowave 300-Anton Paar) was used to carry out the reactions under microwave irradiation in a closed system. Reagent-grade hexane, toluene, THF, ethyl acetate, dioxane, ACN, and DMSO were used as the solvent for the photophysical characterization. Absorption and emission spectra were measured using quartz cuvettes (1 cm path length) on Shimadzu 1800 and Horiba Fluoromax 4 spectrophotometers, respectively.

2.2 Procedure for the synthesis of compounds 3a–f

In a 10 mL microwave vessel, the triethyl phosphonoacetate (1.0 equiv.), the corresponding aldehyde (0.7 equiv.), and potassium carbonate (1.0 equiv.) were dissolved in ethanol (3 mL). The reaction mixture was heated under microwave irradiation at 140 °C for 20 min. Next, the microwave-vessel was cooled at room temperature and the solvent was removed under vacuum. The crude product was purified by column chromatography using a mixture of EtOAc/Hex (4 : 6) as eluents or by crystallization using EtOAc.

2.2.1 Synthesis of ethyl (*E*)-3-(4-(diethylamino)phenyl) acrylate (3a). Yellow oil (0.86 mg, 78%). ^{1}H NMR (400 MHz, $CDCl_3$): δ 1.17 (t, J = 7.1 Hz, 6H, ($\mathbf{CH_3}CH_2$)N), 1.32 (t, J = 7.1 Hz, 3H, $OCH_2\mathbf{CH_3}$), 3.38 (q, J = 7.1 Hz, 4H, ($CH_3\mathbf{CH_2}$)N), 4.23 (q, J = 7.1 Hz, 2H, $O\mathbf{CH_2}CH_3$), 6.19 (d, J = 15.8 Hz, 1H, **CH**C=O), 6.62 (d, J = 8.9 Hz, 2H, H_{arom}), 7.39 (d, J = 8.9 Hz, 2H, H_{arom}), 7.61 (d, J = 15.8 Hz, 1H, =**CH**C_6H_4). ^{13}C NMR (100 MHz, $CDCl_3$): δ 12.6, 14.4, 44.4, 60.0, 111.2, 111.8, 121.4, 130.0, 145.2, 149.3, 168.1 (C=O). HRMS (ESI$^+$) m/z calculated for $C_{15}H_{22}NO_2$ [M + H]$^+$ 248.16505, found 248.16563.[38]

2.2.2 Synthesis of ethyl (*E*)-3-(4-(diphenylamino)phenyl) acrylate (3b). Yellow oil (1.14 g, 76%). ^{1}H NMR (400 MHz, $CDCl_3$): δ 1.32 (t, J = 7.1 Hz, 3H, $\mathbf{CH_3}CH_2O$), 4.24 (q, J = 7.1 Hz, 2H, $O\mathbf{CH_2}CH_3$), 6.28 (d, J = 15.9 Hz, 1H, **CH**C=O), 6.98 (d, J = 8.7 Hz, 2H, $\mathbf{H_{arom}}$), 7.06–7.11 (m, 6H, $\mathbf{H_{arom}}$), 7.24–7.28 (m, 4H, $\mathbf{H_{arom}}$), 7.34 (d, J = 8.7 Hz, 2H, $\mathbf{H_{arom}}$), 7.62 (d, J = 15.9 Hz, 1H, =**CH**C_6H_4). ^{13}C NMR (100 MHz, $CDCl_3$): δ 14.4, 60.3, 115.5, 121.8, 124.0, 125.4, 127.6, 129.2, 129.5, 144.2, 147.0, 149.8, 167.4 (C=O). HRMS (ESI$^+$) m/z calculated for $C_{23}H_{22}NO_2$ [M + H]$^+$ 344.16505, found 344.16477.[42]

2.2.3 Synthesis of diethyl 3,3′-(1,4-phenylene)(2*E*,2′*E*)-diacrylate (3c). White solid (1.18 g, 96%), mp 90–92 °C. ^{1}H NMR (400 MHz, $CDCl_3$): δ 1.34 (t, J = 7.1 Hz, 6H, ($OCH_2\mathbf{CH_3}$)$_2$), 4.27 (q, J = 7.1 Hz, 4H, ($O\mathbf{CH_2}CH_3$)$_2$), 6.47 (d, J = 16.0 Hz, 2H, **CH**C=O), 7.54 (s, 4H, $\mathbf{H_{arom}}$), 7.66 (d, J = 16.0 Hz, 2H, =**CH**C_6H_4). ^{13}C NMR (100 MHz, $CDCl_3$): δ 14.3, 60.6, 119.3, 128.5, 136.1, 143.4, 166.7 (C=O). HRMS (ESI$^+$) m/z calculated for $C_{16}H_{19}O_4$ [M + H]$^+$ 275.12833, found 275.12751.[43]

2.2.4 Synthesis of ethyl (*E*)-3-(4-morpholinophenyl)acrylate (3d). White solid (0.90 g, 77%), mp 128–131 °C, ^{1}H NMR (400 MHz, $CDCl_3$): δ 1.33 (t, J = 7.1 Hz, 3H, $\mathbf{CH_3}CH_2O$), 3.23 (t, J = 4.8 Hz, 4H, ($\mathbf{CH_2}$)$_2$N), 3.85 (t, J = 4.8 Hz, 4H, ($\mathbf{CH_2}$)$_2$O), 4.24 (q, J = 7.1 Hz, 2H, ($CH_3\mathbf{CH_2}O$)), 6.28 (d, J = 15.9 Hz, 1H, **CH**C=O), 6.86 (d, J = 8.8 Hz, 2H, $\mathbf{H_{arom}}$), 7.44 (d, J = 8.8 Hz, 2H, $\mathbf{H_{arom}}$), 7.62 (d, J = 15.9 Hz, 1H, =**CH**C_6H_4). ^{13}C NMR (100 MHz, $CDCl_3$): δ 14.4, 48.2, 60.2, 66.7, 114.7, 125.5, 129.5, 132.2, 144.4, 152.5, 167.5 (C=O). HRMS (ESI$^+$) m/z calculated for $C_{15}H_{20}NO_3$ [M + H]$^+$ 262.14432, found 262.14483.[38]

2.2.5 Synthesis of ethyl (*E*)-3-(4-acetamidophenyl)acrylate (3e). White solid (0.88 g, 84%), mp 130–132 °C. ^{1}H NMR (400 MHz, $CDCl_3$): δ 1.34 (t, J = 7.1 Hz, 3H, $OCH_2\mathbf{CH_3}$), 2.19 (s, 3H, $\mathbf{CH_3}C$=O), 4.26 (q, J = 7.1 Hz, 2H, $O\mathbf{CH_2}CH_3$), 6.35 (d, J = 16.0 Hz, 1H, **CH**C=O), 7.45 (d, J = 8.5 Hz, 2H, $\mathbf{H_{arom}}$), 7.58 (d, J = 8.5 Hz, 2H, $\mathbf{H_{arom}}$), 7.62 (d, J = 16.0 Hz, 1H, **CH**C_6H_4), 8.37 (s, 1H, **NH**C=O). ^{13}C NMR (100 MHz, $CDCl_3$): δ 14.3, 24.4, 60.6, 117.0, 119.9, 129.0, 130.0, 140.0, 144.1, 167.4 (C=O), 169.0 (C=O). HRMS (ESI$^+$) m/z calculated for $C_{13}H_{16}NO_3$ [M + H]$^+$ 234.1130, found 234.1146.[43]

2.2.6 Synthesis of ethyl (*E*)-3-(3,4,5-trimethoxyphenyl)acrylate (3f). White solid (0.87 g, 73%), mp 65–67 °C. ^{1}H NMR (400 MHz, $CDCl_3$): δ 1.35 (t, J = 7.1 Hz, 3H, $OCH_2\mathbf{CH_3}$), 3.88 (s, 3H, $\mathbf{CH_3}O$), 3.89 (s, 6H, ($\mathbf{CH_3}O$)$_2$), 4.27 (q, J = 7.1 Hz, 2H, $O\mathbf{CH_2}CH_3$), 6.36 (d, J = 15.9 Hz, 1H, **CH**C=O), 6.76 (s, 2H, $\mathbf{H_{arom}}$), 7.61 (d, J = 15.9 Hz, 1H, **CH**C_6H_2). ^{13}C NMR (100 MHz, $CDCl_3$): δ 14.4, 56.1, 60.4, 61.0, 105.1, 117.5, 130.0, 140.0, 144.6, 153.4, 167.0

© 2024 The Author(s). Published by the Royal Society of Chemistry

Open Access Article. Published on 11 January 2024. Downloaded on 11/12/2024 6:21:54 AM.
This article is licensed under a Creative Commons Attribution-NonCommercial 3.0 Unported Licence.

(C=O). HRMS (ESI$^+$) m/z calculated for $C_{14}H_{19}O_5$ $[M + H]^+$ 267.12325, found 267.12294.[44]

2.3 Cell bioimaging and *in vitro* cytotoxicity

To study the effect over cell viability of the compounds **3a** and **3b**, and their cellular localization, the Vero cell line (ATCC® CCL-81) was used. Cells were cultured in DMEM medium supplemented with 4 mM L-glutamine, 10% FBS, penicillin (100 IU per mL), and streptomycin (100 mg mL^{-1}) at 37 °C in a 5% CO_2 atmosphere. From each compound, stock solutions of 1 mg mL^{-1} in DMSO were prepared. Working solutions diluted in culture medium were prepared from these stocks and sterilized by filtration (0.2 μm). The final concentration of DMSO was 0.5% or lower. Afterwards, Vero cells were seeded in 96-well tissue culture plates with 5×10^3 cells per well in 100 μL of culture medium, after 24 h of incubation they were supplemented by triplicate with 100 μL of solution of each compound at final concentrations of 0.2, 2, 20 μg mL^{-1}; followed by additional incubation for 24 h. Cell viability was evaluated by WST-1 assay along by light microscopy. To determine intracellular fluorescence of the compounds, Vero cells were seeded in 24-well plates at a density of 2×10^4 cells per well in DMEM supplemented medium at 37 °C, 5% CO_2. After 24 h, the medium was replaced with new medium containing compounds **3a** and **3b** at 25 μg mL^{-1} and incubated for 2 h. Cells were washed with PBS once and imaged using an inverted fluorescence microscopy. Untreated (with cell culture only) and treated cells with the solvent DMSO were used as controls. For statistical analysis, data were analyzed with Student's *t*-test using SPSS version 20.0 software. Additionally, to contrast the intracellular distribution of compounds **3a** and **3b**, a double fluorescent staining was performed using DAPI, a nuclear probe. Vero cells (25 000) were seeded on sterile glass coverslips placed in 24-well microplates with 1 mL of DMEM supplemented medium and incubated for 24 h in a 5% CO_2/95% O_2 atmosphere. After the incubation time, the compounds were added independently at a concentration of 25 μg mL^{-1} and incubated for an additional 2 h. Subsequently, two washes with PBS were performed to remove excess medium, and the coverslips were mounted on glass coverslides, using VECTASHIELD® mounting medium containing DAPI. The slides were observed using an AxioScope A1 microscope (Zeiss, Göttingen, Germany) with a 100× objective and coupled to an Axiocam 502 mono camera coupled to Zen blue software (version 3.3.89.0000). Images were acquired with an Axiophot HXP 120 V fluorescence lamp with the corresponding Zeiss filters.

3. Results and discussion

Cinnamates **3a–f** were prepared in an easy way applying the widely known HWE reaction[45–47] using triethyl phosphonoacetate **1** as the starting material, and commercially available aryl aldehydes **2a–f** [4-(diethylamino)benzaldehyde, 4-(diphenylamino)benzaldehyde, terephthaldehyde, 4-(4-morpholinyl)benzaldehyde, 4-acetamidobenzaldehyde, and 3,4,5-trimethoxybenzaldehyde] using K_2CO_3 as base and ethanol as solvent, under microwave irradiation at 140 °C for 20 min. After purification either by chromatography column or crystallization, the compounds **3a–f** were obtained predominantly as *E* isomers with 73% to 96% yields (Scheme 1). Under these conditions, it was possible to obtain the desired compounds in a one-step reaction, without catalysts, and with improved yields compared to the ones reported in the literature (for compounds **3a** and **3d**, Y. Mizuta,[38] reported 46% and 49% yield respectively; for compound **3c**, J. Lu,[43] reported 89% yield, for compound **3b**, X. Zeng,[42] reported 97% yield, and for compound **3f**, E. Nomura,[44] reported 66% yield). Therefore, we are now reporting an eco-friendly experimental protocol for the synthesis of these compounds.

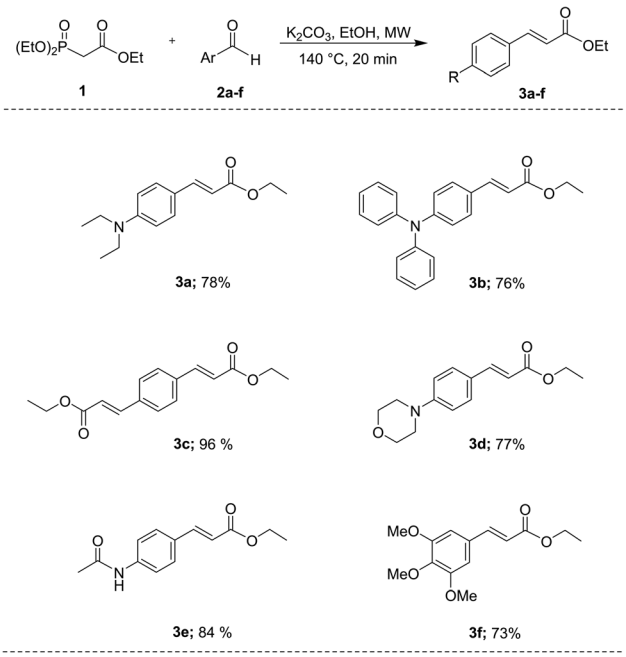

Scheme 1 Preparation of ethyl cinnamates **3a–f**. Yields after purification by column chromatography.

3.1 Photophysical properties

With ethyl cinnamates **3a–f** synthesized and characterized, and in order to obtain information about their photophysical properties, UV-vis absorption and photoluminescent spectra of these compounds in ethyl acetate solutions were initially recorded (Fig. 1). Fig. 1a shows the absorption spectra of compounds **3a–f** (absorbance data were normalized), which are in the range between 260–420 nm, and are attributed to n → π* transitions. The absorption spectra of compounds **3a–f** shown wavelengths of maximum absorption (λ_{abs}) at 366, 370, 316, 339, 314, and 309 nm, respectively; where the absorption spectrum of **3a** is similar to **3b**, being these two compounds red-shifted. Fig. 1b shows the photoluminescent spectra for compounds **3a–f**, where the compounds **3a** and **3c–f** exhibit blue emissions with maximum intensities in the range of 369–442 nm.

It is noteworthy, that compound **3b** exhibits blue-green emission at 504 nm, which had a bathochromic shift by about

Open Access Article. Published on 11 January 2024. Downloaded on 11/12/2024 6:21:54 AM.
This article is licensed under a Creative Commons Attribution-NonCommercial 3.0 Unported Licence.

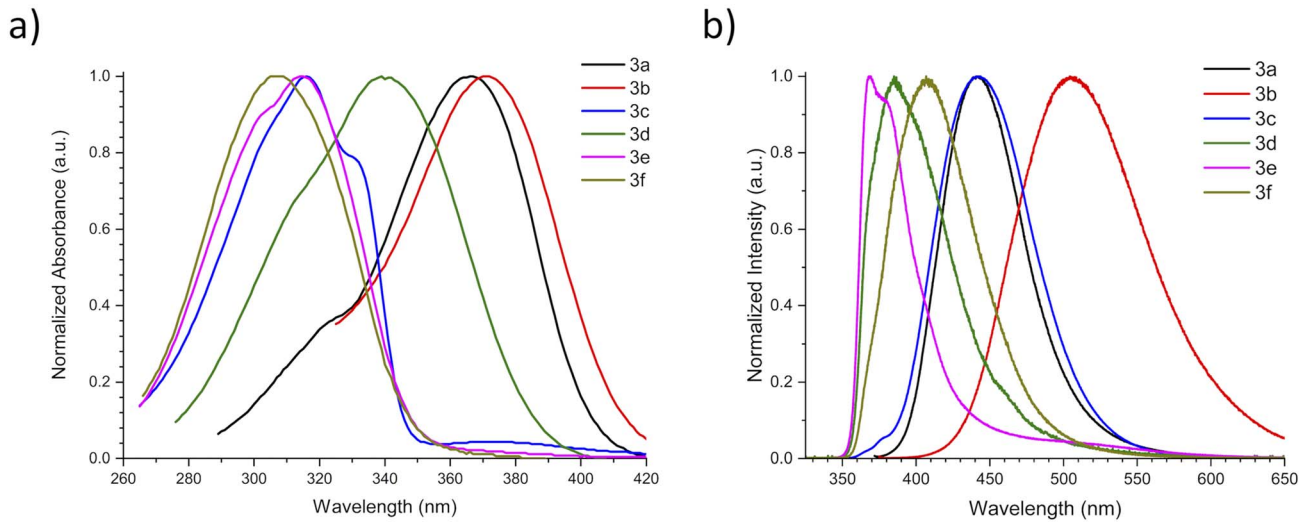

Fig. 1 (a) Absorption and (b) emission spectra of ethyl cinnamates **3a–f**.

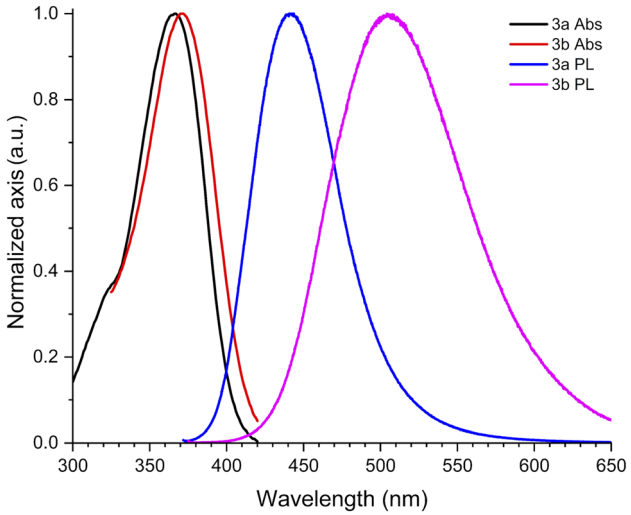

Fig. 2 Absorption and emission spectra of the compounds **3a** and **3b**.

62 nm with respect to **3a**, which has a wavelength of maximum emission (λ_{em}) at 442 nm (Fig. 2). The latter can be attributed to a higher level of conjugation due to the presence of the diphenylamino group, see Table 1. The Stokes shifts (SS) were calculated from the absorption and emission maximum wavelengths for each compound, getting the following values: 76, 134, 126, 46, 55, and 97 nm, showing that compound **3b** has the largest Stokes shift (134 nm).

Fluorescence quantum yields (Φ) of **3a–f** in ethyl acetate were measured using quinine sulphate ($\Phi_R = 0.55$ in H_2SO_4, 0.05 M) as reference by a comparative method:[48]

$$\Phi = \frac{I\left(1-10^{-A_R}\right)n^2}{I_R\left(1-10^{-A}\right)n_R{}^2} \times \Phi_R \times 100 \quad (1)$$

where subscript R indicates values related to the standard, A is the absorbance value at the excitation wavelength, I is the area under the emission spectrum curve, and n is the refractive index of the solvent used. The Φ values obtained are the following: 1.4%, 17.8%, 1.2%, 0.77%, 0.8%, 1.1%, highlighting again the compound **3b** with the highest value (17.8%). The emission of the compounds **3a**, **3b**, and **3f** is shown in the CIE chromaticity diagram of Fig. SI19,† and the coordinates (x,y) with the emission data in Table 1. The blue-green emission of compound **3b** can be observed in Fig. 3.

In spite of their similar λ_{abs} values, compounds **3a** and **3b** show significantly different λ_{em} and the Φ value of **3b** is around 12 times larger than that of **3a**. This behavior can be attributed to the biphenyl's chromophore present in **3b**.

Based on the photophysical properties results using ethyl acetate as solvent, it was decided to perform a more detailed

Table 1 Summary of photophysical properties of **3a–f**

Compound	λ_{abs} (nm)	E_{abs} (eV)	ε (10^4 M^{-1} cm^{-1})	λ_{em} (nm)	E_{em} (eV)	SS (nm)	SS (eV)	Φ (%)	CIE (x,y)
3a	366	3.39	3.06	442	2.81	76	0.58	1.4	(0.15,0.07)
3b	370	3.35	3.36	504	2.46	134	0.89	17.8	(0.23,0.43)
3c	316	3.92	2.4	442	2.81	126	1.12	1.2	(0.14,0.07)
3d	339	3.66	1.79	385	3.22	46	0.44	0.77	(0.16,0.06)
3e	314	3.95	1.75	369	3.36	55	0.59	0.8	(0.18,0.15)
3f	309	4.01	1.53	406	3.05	97	0.96	1.1	(0.15,0.04)

© 2024 The Author(s). Published by the Royal Society of Chemistry

Open Access Article. Published on 11 January 2024. Downloaded on 11/12/2024 6:21:54 AM. This article is licensed under a Creative Commons Attribution-NonCommercial 3.0 Unported Licence.

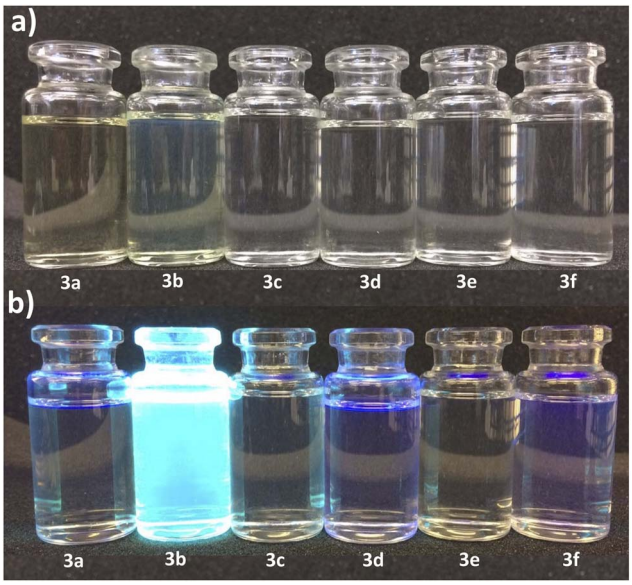

Fig. 3 Solution of compounds **3a–f** under (a) room light and (b) UV radiation at 365 nm.

study of compounds **3a** and **3b**, which presented the best photophysical properties, using a series of solvents of ranging polarity (hexane, toluene, THF, EtOAc, dioxane, ACN, DMSO), see Fig. SI20.† Results showed maximum absorption values between 350–377 nm for **3a** and 363–415 nm for **3b**. In addition, a bathochromic shift was observed when increasing the solvent polarity, which is more noticeable for compound **3b**. On the other hand, the highest molar extinction coefficients were achieved using DMSO as solvent, 37 600 and 40 100 M^{-1} cm^{-1} for **3a** and **3b**, respectively. Whereas both compounds **3a** and **3b** exhibited the lowest values in hexane, 15 900 and 13 500 M^{-1} cm^{-1}, respectively (Table 2 and Fig. 4). This behavior may be attributed to possible compound–solvent interactions.[49]

Furthermore, the emission spectra show a noteworthy red solvatochromic shift as the polarity of the solvent increases. This could be attributed to the intramolecular charge transfer.[50,51] Additionally, the quantum yield analysis in solution exhibited higher values using DMSO ($\Phi = 2.1\%$) and ACN ($\Phi = 19.3\%$) for **3a** and **3b**, respectively, noting a quite linear decline in fluorescence intensity, as the solvent polarity decreases. The decreasing trend in quantum yield in non-polar solvents may be attributed to the slight difference between their ground and excited states.[52–54] Moreover, SS values above 100 nm were found for compound **3b** in THF, EtOAc, dioxane, ACN, and DMSO (Table 2 and Fig. 4).

In addition to quantum yield and Stokes shifts, to evaluate the eligibility of a compound for fluorescent cell imaging, the extinction coefficient (ε) is also a determining parameter. In this respect, **3a** and **3b** showed ε values > 30 000 M^{-1} cm^{-1} in all tested solvents except hexane and toluene, making them appropriate for medical and biological applications.[14] Based on these results, we selected the derivatives **3a** and **3b** to be evaluated as fluorescent cell dyes due to the combination of their noticeable chemical yield, quantum yield, Stokes shift, and extinction coefficient values.

3.2 Theoretical calculations

Geometry optimizations and TDDFT calculations were performed to determine the ground state structure for all synthesized compounds, and to obtain the electronic spectra to study the S_0–S_1 transition. The calculated wavelength absorption maxima are all in good agreement with the experimental measurements in ethyl acetate.[55]

The HOMO–LUMO frontier molecular orbitals of the compounds **3a–3f** in ethyl acetate as solvent are summarized in Table 3. For **3a** and **3b**, there are similar donating portions where the amine is donating electron density to the pi-bridging phenyl ring. While in **3a** the diethyl portion hyperconjugates to enhance donation from the amine, in **3b** the two additional aromatic rings provide what could be assigned as the highest donated electron density, which would be discernible as the most red-shifted absorption, as corroborated experimentally.

Table 2 Summary of photophysical properties of compounds **3a–b** in solution[a]

Solvent	λ_{abs} (nm)	E_{abs} (eV)	ε (10^4 M^{-1} cm^{-1})	λ_{em} (nm)	E_{em} (eV)	SS (nm)	Φ (%)
DMSO	377	3.29	3.76	454	2.73	82	2.1
	415[a]	2.99[a]	4.01[a]	537[a]	2.31[a]	122[a]	19.01[a]
ACN	369	3.36	3.35	452	2.74	81	1.8
	409[a]	3.03[a]	3.89[a]	531[a]	2.33[a]	122[a]	19.3[a]
Dioxane	366	3.39	3.22	445	2.79	80	1.9
	380[a]	3.26[a]	3.41[a]	515[a]	2.40[a]	135[a]	18.6[a]
EtOAc	366	3.39	3.06	442	2.81	76	1.4
	370[a]	3.35[a]	3.36[a]	504[a]	2.46[a]	134[a]	17.8[a]
THF	367	3.37	3.01	420	2.95	57	1.1
	375[a]	3.30[a]	3.39[a]	487[a]	2.55[a]	112[a]	15.7[a]
Toluene	371	3.34	2.68	408	3.04	37	0.87
	368[a]	3.37[a]	2.75[a]	443[a]	2.80[a]	75[a]	3.9[a]
Hexane	350	3.54	1.59	398	3.11	45	0.44
	363[a]	3.41[a]	1.35[a]	404[a]	3.07[a]	41[a]	2.4[a]

[a] Data for compound **3b**.

Open Access Article. Published on 11 January 2024. Downloaded on 11/12/2024 6:21:54 AM.
This article is licensed under a Creative Commons Attribution-NonCommercial 3.0 Unported Licence.

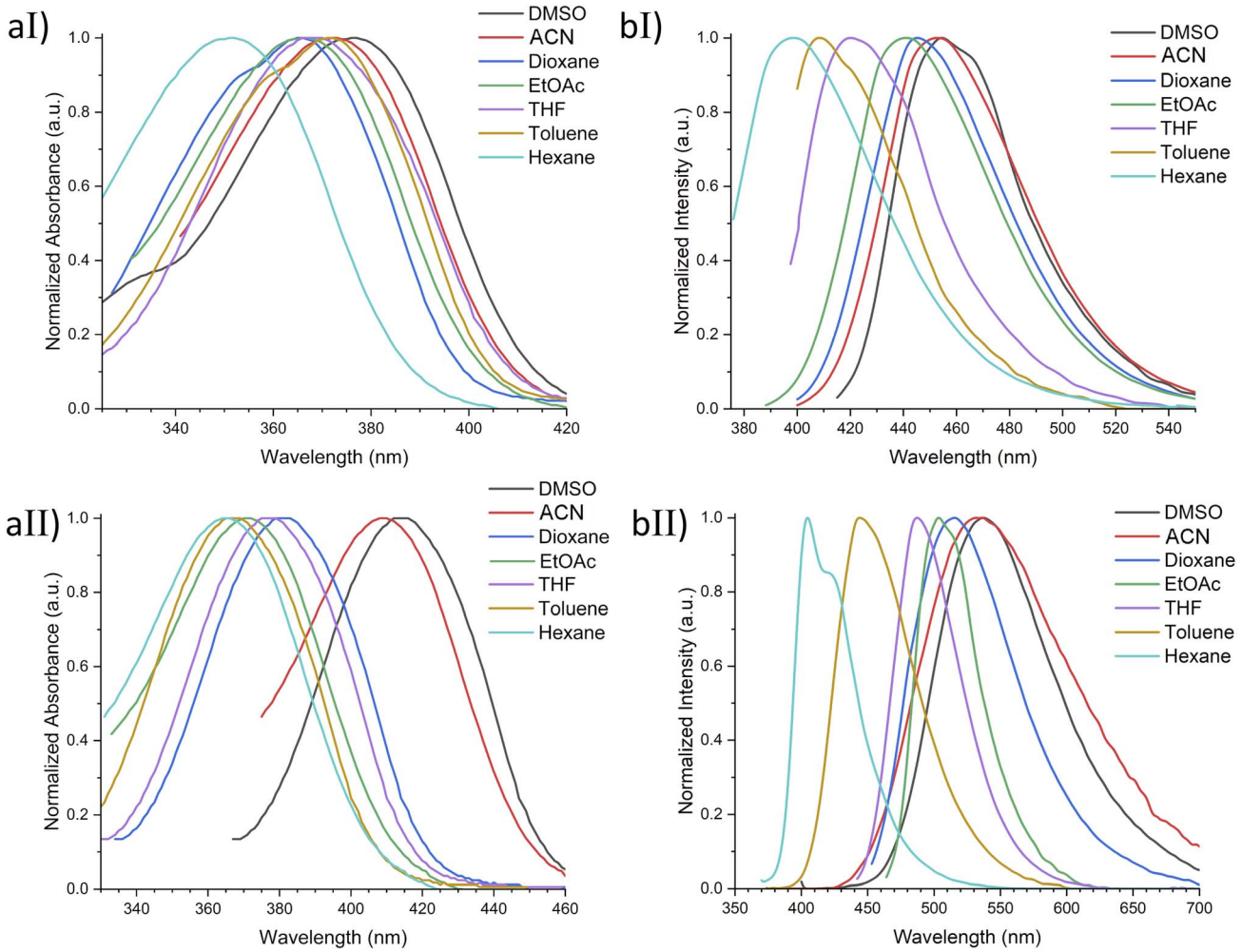

Fig. 4 (a) Absorption and (b) emission spectra of compounds **3a** (I) and **3b** (II) in solution.

Compound **3d** has a somewhat similar behavior where the cyclic amine donates electron density but having the oxygen atom incorporated in the morpholine cycle reduces the available delocalization, compared to what is observed for **3a** and **3b**.

The ethyl acrylate group in **3c** and the double-bond character of the amide group in **3e** can be rationalized as having similar electronic properties and provide very similar delocalization of electron density towards the π-bridge portion.

Compound **3f** only shows donation towards the phenyl ring, stemming from the methoxy portions, whose group electronegativity do not allow a strong donating effect. This is reflected in the lowest maximum wavelength of the series.

Finally, we can observe a quinoid delocalization from the phenyl to the acrylate portion which is shared in the whole series producing the "pull" effect on the studied molecules.

The electronic nature of the transition in the whole series has as consequence that their S_0–S_1 transition present a HOMO–LUMO character in more than 90% (Fig. 5).

Table 3 Absorption maxima λ_{max} (nm), excitation energy E (eV), oscillator strength (f), and molecular orbitals contribution (%), calculated at CAM-B3LYP/6-311+G level

Compound	State	E (eV)	λ_{max} (nm)	f	Assignment	Exp.[a] (nm)
3a	S1	3.69	335.6	1.1350	HOMO–LUMO (95%)	366
3b	S1	3.54	349.8	1.0310	HOMO–LUMO (90%)	370
3c	S1	3.91	317.1	1.5055	HOMO–LUMO (96%)	316
3d	S1	3.82	324.1	1.1273	HOMO–LUMO (94%)	339
3e	S1	4.14	299.2	1.1085	HOMO–LUMO (96%)	314
3f	S1	4.39	281.9	0.9083	HOMO–LUMO (95%)	309

[a] Results obtained in ethyl acetate as solvent.

© 2024 The Author(s). Published by the Royal Society of Chemistry

Open Access Article. Published on 11 January 2024. Downloaded on 11/12/2024 6:21:54 AM.
This article is licensed under a Creative Commons Attribution-NonCommercial 3.0 Unported Licence.

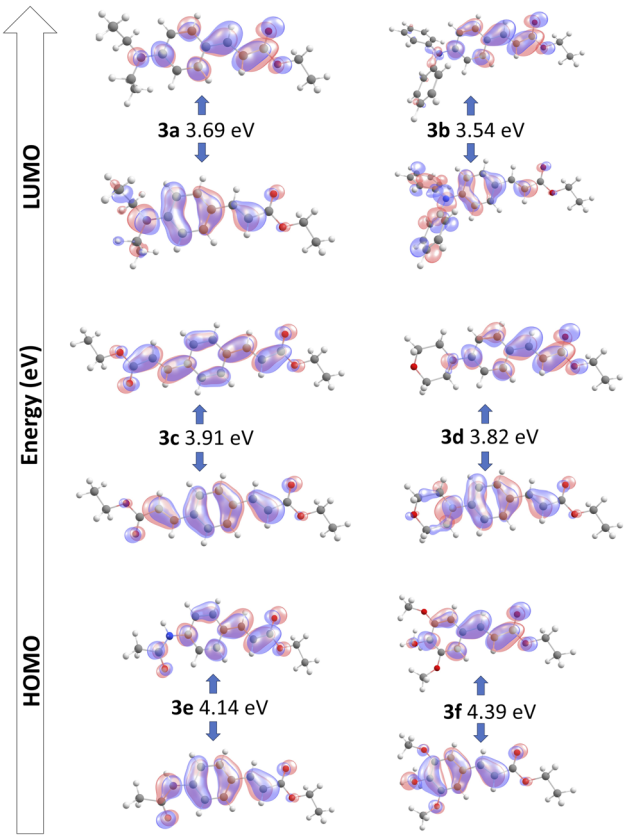

Fig. 5 Frontier molecular orbitals obtained using CAM-B3LYP/6-311+G level.

3.3 Cell bioimaging and *in vitro* cytotoxicity

The cytotoxicity was assessed by the WST-1 assay in Vero cells following a 24 h treatment with the compounds **3a**, **3b** and DMSO as solvent. The results did not show a cytotoxicity effect of compounds **3a** and **3b** even at concentrations of 20 μg mL^{-1}.

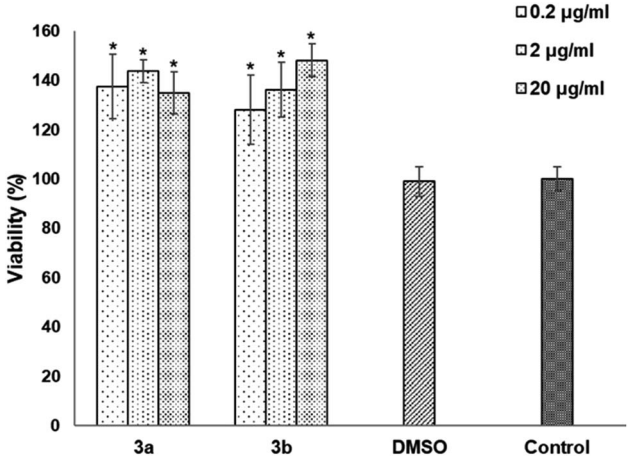

Fig. 6 Effects of compounds **3a** and **3b** over Vero cells viability. Cytotoxic effect was measured by WST-1 assay after 24 h treatment with compounds at 0.2, 2, and 20 μg mL^{-1}. Results from three independent experiments (means ± SD). *$p < 0.05$ *versus* control.

On the contrary, it is striking that an increase of 20–40% in cell proliferation occurs at these doses compared to the viability of the controls (Fig. 6). This behavior could be related to hormesis since, according to a systematic review of 9000 hormetic responses, it was found that the stimulatory effect varies from 30–60% in comparison to the control groups.[56] Hormesis is a biological phenomenon that occurs in a wide variety of species and is induced by different chemical compounds, either natural or synthetic; it is generally accepted that favors adaptation to overcome unfavorable or stressful conditions in the normal environment of different organisms.[57] Regardless of the model, the evaluation criteria, and the inducing agent, the hormetic effect is characterized by stimulation at low doses, while it is inhibitory at high doses.[58] At cellular level, activation of signaling cascades occurs in which transcription and growth factors, kinase and deacetylase enzymes, and antioxidant enzymes have been involved.[59] The latter is particularly important because a wide variety of xenobiotics induce oxidative stress and the hormetic effect has been directly related to the production of reactive oxygen species.[60,61] It has also been reported that exposure to chemical agents induces oxidative stress, which mediated activation of signaling pathways involved in cell proliferation and apoptosis.[62] According to our results, it is possible to suggest that Vero cells were under oxidative stress and possibly increased cell proliferation as an adaptation or physiological alert response in the presence of the studied compounds.

The compounds **3a** and **3b** were also tested as dyes for fluorescence microscopy, using Vero cells as model for studying cellular staining, uptake, and localization. Fig. 7 shows panoramic (a and c) and zoom-in (b and d) images of Vero cell

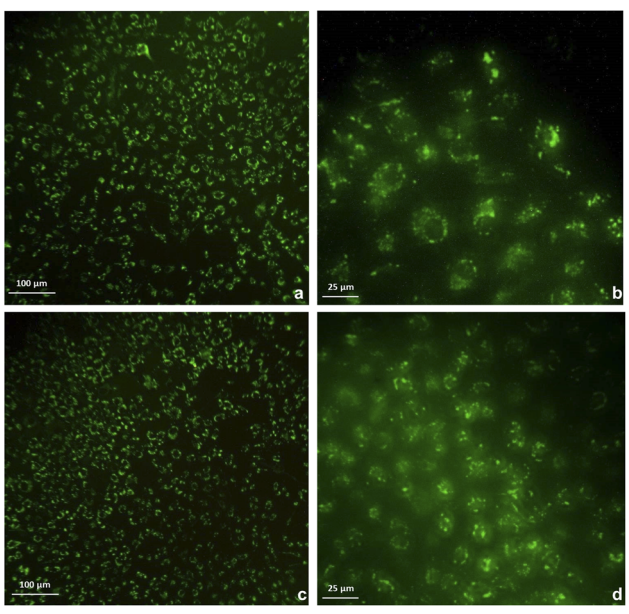

Fig. 7 Staining of Vero cells with compounds **3a** and **3b**. The cells were incubated, for 2 h, with 25 μg mL^{-1} of each compound. Compound **3a** (a and b), and compound **3b** (c and d). Fluorescence microscopy 10× (a and c). 40× (b and d).

Open Access Article. Published on 11 January 2024. Downloaded on 11/12/2024 6:21:54 AM.
This article is licensed under a Creative Commons Attribution-NonCommercial 3.0 Unported Licence.

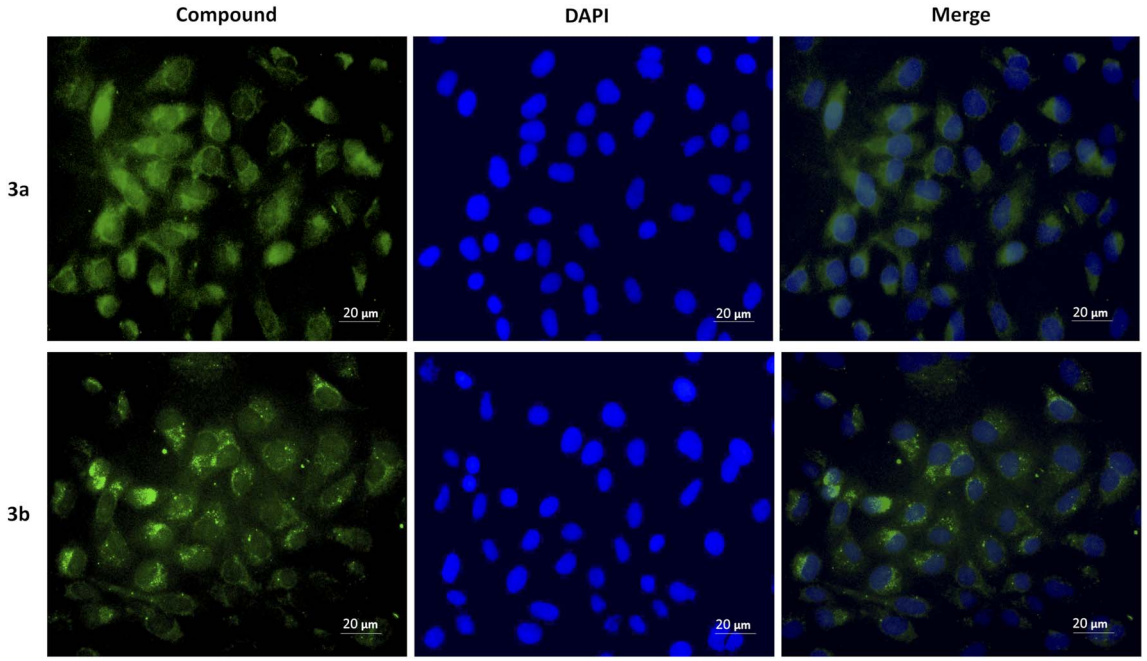

Fig. 8 Representative fluorescence microscopy images of compound **3a** (upper panel) and compound **3b** (lower panel) in Vero cells monolayers. As described in Experimental section, cells were incubated with compounds **3a** and **3b** (left panels) and with DAPI to stain nuclei (middle panel). Merged images with double staining are shown in the right panel. Magnification: 200×. Scale bars, 20 μm.

monolayers incubated with compounds **3a** (a and b) and **3b** (c and d) in which intracellular fluorescence is observed.

This kind of dyes have shown to be largely internalized by cells *via* endocytosis. The microscopic approach allows us to observe that the fluorescent staining is selective, and that compound **3a** stains the cytoplasm of the cells, while compound **3b** stains the nucleoli, which are seen as solid spots of intense fluorescence, while the cytoplasm is observed as a fined shadow around the nuclei.

To demonstrate the intracellular localization of compounds **3a** and **3b**, a double fluorescent staining was performed using these compounds and DAPI, which stains blue the cell nuclei and allows to appreciate that compound **3a** produces diffuse cytoplasmic staining, while compound **3b** accumulates around the nuclei (Fig. 8).

4. Conclusions

In summary, a simple and eco-friendly microwave-assisted organic synthesis, for the preparation of ethyl cinnamates, has been successfully performed with good chemical yields, *via* Horner–Wadsworth–Emmons reaction. The photophysical properties demonstrated that compounds **3a** and **3c–f** presented low fluorescence quantum yields from 0.77% to 1.4%, while compound **3b** presented the highest value (17.8%) using EtOAc as solvent. Likewise, compound **3b** showed the largest Stokes shift (135 nm) using dioxane as solvent. Compounds **3a** and **3b** showed ε values > 30 000 M^{-1} cm^{-1} in all tested solvents except hexane and toluene. Based on these last properties, compounds **3a** and **3b** were selected to assess their cytotoxicity, at different concentrations, using Vero cells. The results evidenced that the compounds **3a** and **3b** were not cytotoxic and they were internalized by cells; showing that compound **3a** stains the cytoplasm, and compound **3b** stains the nuclei in a selective way. Besides, these studies demonstrated that compounds **3a** and **3b** could be used as fluorescent dyes for biological and medical applications.

Conflicts of interest

The authors declare that there are no conflicts of interest in this work.

Acknowledgements

The authors thank CONAHCYT of Mexico for the financial support, with grant number CB-2015/256359. MAAM and ELPN also thank CONACYT for the scholarships 596332 and 888781.

References

1 D. N. Kanekar, S. Chacko and R. M. Kamble, Quinoxaline Based Amines as Blue-Orange Emitters: Effect of Modulating Donor System on Optoelectrochemical and Theoretical Properties, *Dyes Pigm.*, 2019, **167**, 36–50, DOI: 10.1016/J.DYEPIG.2019.04.005.

2 V. V. Utochnikova, N. N. Solodukhin, A. N. Aslandukov, L. Marciniak, I. S. Bushmarinov, A. A. Vashchenko and N. P. Kuzmina, Lanthanide Tetrafluorobenzoates as Emitters for OLEDs: New Approach for Host Selection, *Org. Electron.*, 2017, **44**, 85–93, DOI: 10.1016/j.orgel.2017.01.026.

© 2024 The Author(s). Published by the Royal Society of Chemistry

Open Access Article. Published on 11 January 2024. Downloaded on 11/12/2024 6:21:54 AM. This article is licensed under a Creative Commons Attribution-NonCommercial 3.0 Unported Licence.

3 S.-H. Jeong, K. H. Lee and J. Y. Lee, Dual Role of a Pyrene Derivative as a Hole Transport Material and an Emitter in Blue Fluorescent Organic Light-Emitting Diodes, *Dyes Pigm.*, 2019, **171**, 107759, DOI: 10.1016/J.DYEPIG.2019.107759.

4 L. Yan, R. Li, W. Shen and Z. Qi, Multiple-Color AIE Coumarin-Based Schiff Bases and Potential Application in Yellow OLEDs, *J. Lumin.*, 2018, **194**, 151–155, DOI: 10.1016/j.jlumin.2017.10.032.

5 K. S. Daskalakis, F. Freire-Fernández, A. J. Moilanen, S. Van Dijken and P. Törmä, Converting an Organic Light-Emitting Diode from Blue to White with Bragg Modes, *ACS Photonics*, 2019, **6**, 2655–2662, DOI: 10.1021/acsphotonics.9b01206.

6 J. Huang, L. Liu, Y. Peng, Y. Fu, Z. Song, C. Zhong, J. Yang, J. Zhou, Y. Zhang, Y. Luo, *et al.*, Design of a Quinazolinone-Based Environment-Sensitive Fluorescent Dye: Solvatochromic Fluorescence and Application for One-Photon and Two-Photon Bioimaging, *Dyes Pigm.*, 2019, **165**, 58–64, DOI: 10.1016/j.dyepig.2019.01.051.

7 X. Wu and W. Zhu, Stability Enhancement of Fluorophores for Lighting up Practical Application in Bioimaging, *Chem. Soc. Rev.*, 2015, **44**, 4179–4184, DOI: 10.1039/c4cs00152d.

8 S. Reimann, M. Sharif, K. Wittler, L. R. Knöpke, A. E. Surkus, C. Roth, R. Ludwig and P. Langer, 3-Pyrenylacrylates: Synthetic, Photophysical, Theoretical and Electrochemical Investigations, *Z. Naturforsch., C: J. Biosci.*, 2013, **68**, 367–377, DOI: 10.5560/znb.2013-3004.

9 G. Sathiyan, E. K. T. Sivakumar, R. Ganesamoorthy, R. Thangamuthu and P. Sakthivel, Review of Carbazole Based Conjugated Molecules for Highly Efficient Organic Solar Cell Application, *Tetrahedron Lett.*, 2016, **57**, 243–252, DOI: 10.1016/j.tetlet.2015.12.057.

10 U. M. V. Basavanag, A. Islas-Jácome, A. Rentería-Gómez, A. S. Conejo, M. Kurva, J. O. C. Jiménez-Halla, J. Velusamy, G. Ramos-Ortíz and R. Gámez-Montaño, Synthesis of 2-Julolidin-Imidazo[1,2-a] Pyridines via Groebke-Blackburn-Bienaymé Reaction and Studies of Optical Properties, *New J. Chem.*, 2017, **41**, 3450–3459, DOI: 10.1039/c6nj04044f.

11 M. Srinivas, G. R. Vijayakumar, K. M. Mahadevan, H. Nagabhushana and H. S. Bhojya Naik, Synthesis, Photoluminescence and Forensic Applications of Blue Light Emitting Azomethine-Zinc(II) Complexes of Bis(Salicylidene)Cyclohexyl-1,2-Diamino Based Organic Ligands, *J. Sci.: Adv. Mater. Devices*, 2017, **2**, 156–164, DOI: 10.1016/j.jsamd.2017.02.008.

12 G. Attia, S. Rahali, S. Teka, N. Fourati, C. Zerrouki, M. Seydou, S. Chehimi, S. Hayouni, J. P. Mbakidi, S. Bouquillon, *et al.*, Anthracene Based Surface Acoustic Wave Sensors for Picomolar Detection of Lead Ions. Correlation between Experimental Results and DFT Calculations, *Sens. Actuators, B*, 2018, **276**, 349–355, DOI: 10.1016/j.snb.2018.08.033.

13 J. Sun, P. Cai, X. Zhang, A. Liang, L. Zhang and J. Chen, Synthesis, Characterization and Device Application of a Novel Blue-Emitting Copolymer Incorporating Fluorene and Benzothiazole Backbone Units, *Opt. Mater.*, 2019, **98**, 109443, DOI: 10.1016/J.OPTMAT.2019.109443.

14 W. Wang, H. Mattoussi, A. Kapur, G. Palui, S. H. Medina, X. Ji and J. P. Schneider, Enhanced Uptake of Luminescent Quantum Dots by Live Cells Mediated by a Membrane-Active Peptide, *ACS Omega*, 2018, **3**, 17164–17172, DOI: 10.1021/acsomega.8b02918.

15 X. Y. Shen, W. Z. Yuan, Y. Liu, Q. Zhao, P. Lu, Y. Ma, I. D. Williams, A. Qin, J. Z. Sun and B. Z. Tang, Fumaronitrile-Based Fluorogen: Red to near-Infrared Fluorescence, Aggregation-Induced Emission, Solvatochromism, and Twisted Intramolecular Charge Transfer, *J. Phys. Chem. C*, 2012, **116**, 10541–10547, DOI: 10.1021/jp303100a.

16 J. Yao, M. Yang and Y. Duan, Chemistry, Biology, and Medicine of Fluorescent Nanomaterials and Related Systems: New Insights into Biosensing, Bioimaging, Genomics, Diagnostics, and Therapy, *Chem. Rev.*, 2014, **114**, 6130–6178, DOI: 10.1021/cr200359p.

17 A. S. Ortega-Villarreal, E. Hernández-Fernández, C. Jensen, G. A. Valdivia-Berroeta, S. Garrard, I. López, S. J. Smith, K. A. Christensen, M. A. Reyes-González and D. J. Michaelis, Synthesis and Characterization of Ethyl Benzotriazolyl Acrylate-Based D-π-A Fluorophores for Live Cell-Based Imaging Applications, *RSC Adv.*, 2019, **9**, 8759–8767, DOI: 10.1039/c9ra00108e.

18 P. Khanna and P. C. Basak, An OER Architecture Framework: Needs and Design, *Int. Rev. Res. Open Distance Learn.*, 2013, **14**, 65–83, DOI: 10.1016/j.rser.2012.02.021.

19 S. W. Yun, N. Y. Kang, S. J. Park, H. H. Ha, Y. K. Kim, J. S. Lee and Y. T. Chang, Diversity Oriented Fluorescence Library Approach (DOFLA) for Live Cell Imaging Probe Development, *Acc. Chem. Res.*, 2014, **47**, 1277–1286, DOI: 10.1021/ar400285f.

20 L. Zhao, S. Wang, J. Ding and L. Wang, Solution-Processible Blue Fluorescent Dendrimers with Carbazole/Diphenylamine Hybrid Dendrons for Power-Efficient Organic Light-Emitting Diodes, *ACS Omega*, 2019, **4**, 15923–15928, DOI: 10.1021/acsomega.9b01979.

21 V. I. Martynov, A. A. Pakhomov, N. V. Popova, I. E. Deyev and A. G. Petrenko, Synthetic Fluorophores for Visualizing Biomolecules in Living Systems, *Acta Nat.*, 2016, **8**, 33–46, DOI: 10.32607/20758251-2016-8-4-33-46.

22 Z. Wang, S. Chen, J. W. Y. Lam, W. Qin, R. T. K. Kwok, N. Xie, Q. Hu and B. Z. Tang, Long-Term Fluorescent Cellular Tracing by the Aggregates of AIE Bioconjugates, *J. Am. Chem. Soc.*, 2013, **135**, 8238–8245, DOI: 10.1021/ja312581r.

23 J. Zhang, R. Chen, Z. Zhu, C. Adachi, X. Zhang and C. S. Lee, Highly Stable Near-Infrared Fluorescent Organic Nanoparticles with a Large Stokes Shift for Noninvasive Long-Term Cellular Imaging, *ACS Appl. Mater. Interfaces*, 2015, **7**, 26266–26274, DOI: 10.1021/acsami.5b08539.

24 Y. Yang, Q. Zhao, W. Feng and F. Li, Luminescent Chemodosimeters for Bioimaging, *Chem. Rev.*, 2013, **113**, 192–270, DOI: 10.1021/cr2004103.

25 J. Goedhart, D. Von Stetten, M. Noirclerc-Savoye, M. Lelimousin, L. Joosen, M. A. Hink, L. Van Weeren, T. W. J. Gadella and A. Royant, Structure-Guided Evolution of Cyan Fluorescent Proteins towards a Quantum Yield of

Open Access Article. Published on 11 January 2024. Downloaded on 11/12/2024 6:21:54 AM. This article is licensed under a Creative Commons Attribution-NonCommercial 3.0 Unported Licence.

93%, *Nat. Commun.*, 2012, **3**, 751, DOI: 10.1038/ncomms1738.

26 S. W. Thomas, G. D. Joly and T. M. Swager, Chemical Sensors Based on Amplifying Fluorescent Conjugated Polymers, *Chem. Rev.*, 2007, **107**, 1339–1386, DOI: 10.1021/cr0501339.

27 C. C. Cheng, Z. S. Liao, J. J. Huang, D. J. Lee and J. K. Chen, Supramolecular Polymer Micelles as Universal Tools for Constructing High-Performance Fluorescent Nanoparticles, *Dyes Pigm.*, 2017, **137**, 284–292, DOI: 10.1016/j.dyepig.2016.10.028.

28 K. H. Lee and J. Y. Lee, Paradigm Change of Blue Emitters: Thermally Activated Fluorescence Emitters as Long-Living Fluorescence Emitters by Triplet Exciton Quenching, *Org. Electron.*, 2019, **75**, 105377, DOI: 10.1016/J.ORGEL.2019.105377.

29 M. Zhu and C. Yang, Blue Fluorescent Emitters: Design Tactics and Applications in Organic Light-Emitting Diodes, *Chem. Soc. Rev.*, 2013, **42**, 4963–4976, DOI: 10.1039/c3cs35440g.

30 M. Lepeltier, X. Sallenave, D. Tondelier, G. Sini, F. Goubard, D. Gigmes, B. Geffroy and F. Dumur, Triphenylamine/Oxadiazole Hybrids Differing by the Substitution Pattern: Influence on the Electroluminescence Properties of Yellow and Green Emitting Diodes, *Synth. Met.*, 2018, **240**, 21–29, DOI: 10.1016/j.synthmet.2018.03.008.

31 M. Aydemir, G. Haykir, A. Battal, V. Jankus, S. K. Sugunan, F. B. Dias, H. Al-Attar, F. Türksoy, M. Tavasli and A. P. Monkman, High Efficiency OLEDs Based on Anthracene Derivatives: The Impact of Electron Donating and Withdrawing Group on the Performance of OLED, *Org. Electron.*, 2016, **30**, 149–157, DOI: 10.1016/j.orgel.2015.11.026.

32 J. Jayabharathi, R. Sathishkumar, V. Thanikachalam and K. Jayamoorthy, High Efficiency, Blue Emitting Materials Based on Phenanthro[9,10-d] Imidazole Derivatives, *J. Lumin.*, 2014, **153**, 343–349, DOI: 10.1016/j.jlumin.2014.03.060.

33 M. Thelakkat and H. W. Schmidt, Low Molecular Weight and Polymeric Heterocyclics as Electron Transport/Hole-Blocking Materials in Organic Light-Emitting Diodes, *Polym. Adv. Technol.*, 1998, **9**, 429–442, DOI: 10.1002/(SICI)1099-1581(199807)9:7<429::AID-PAT798>3.0.CO;2-E.

34 Y. Jia, S. Wu, Y. Zhang, S. Fan, X. Zhao, H. Liu, X. Dong, S. Wang and X. Li, Achieving Non-Doped Deep-Blue OLEDs by Applying Bipolar Imidazole Derivatives, *Org. Electron.*, 2019, **69**, 289–296, DOI: 10.1016/j.orgel.2019.03.044.

35 K. Selvakumar, A. Zapf, A. Spannenberg and M. Beller, Synthesis of Monocarbenepalladium(0) Complexes and Their Catalytic Behavior in Cross-Coupling Reactions of Aryldiazonium Salts, *Chem.–Eur. J.*, 2002, **8**, 3901–3906, DOI: 10.1002/1521-3765(20020902)8:17<3901::AID-CHEM3901>3.0.CO;2-E.

36 C. H. Lo and H. M. Lee, Synthesis and Characterization of C, C-Type Palladacycles and Their Catalytic Application in Mizoroki-Heck Coupling Reaction, *Organometallics*, 2018, **37**, 1150–1159, DOI: 10.1021/acs.organomet.8b00054.

37 M. Moreno-Mañas, M. Pérez and R. Pleixats, Stereospecific Preparation of Ethyl (E) and (Z)-3-Aryl-3-Phenylpropenoates by Heck Reaction, *Tetrahedron Lett.*, 1996, **37**, 7449–7452, DOI: 10.1016/0040-4039(96)01608-5.

38 Y. Mizuta, Y. Obora, Y. Shimizu and Y. Ishii, Para-Selective Aerobic Oxidative C-H Olefination of Aminobenzenes Catalyzed by Palladium/Molybdovanadophosphoric Acid/2,4,6-Trimethylbenzoic Acid System, *ChemCatChem*, 2012, **4**, 187–191, DOI: 10.1002/cctc.201100375.

39 H. Lebel and M. Davi, Diazo Reagents in Copper(I)-Catalyzed Olefination of Aldehydes, *Adv. Synth. Catal.*, 2008, **350**, 2352–2358, DOI: 10.1002/adsc.200800381.

40 B. List, A. Doehring, M. T. Hechavarria Fonseca, A. Job and R. Rios Torres, A Practical, Efficient, and Atom Economic Alternative to the Wittig and Horner-Wadsworth-Emmons Reactions for the Synthesis of (E)-α,β-Unsaturated Esters from Aldehydes, *Tetrahedron*, 2006, **62**, 476–482, DOI: 10.1016/j.tet.2005.09.081.

41 S. Kumar, U. Mabalirajan, R. Rehman, B. K. Singh, V. S. Parmar, A. K. Prasad, S. Biswal and B. Ghosh, A Novel Cinnamate Derivative Attenuates Asthma Features and Reduces Bronchial Epithelial Injury in Mouse Model, *Int. Immunopharmacol.*, 2013, **15**, 150–159, DOI: 10.1016/j.intimp.2012.10.024.

42 X. Zeng, Z. Chen, L. Tang, H. Yang, N. Liu, H. Zhou, Y. Li, J. Wu, Z. Deng, Y. Yu, *et al.*, A Novel Near-Infrared Fluorescent Light-up Probe for Tumor Imaging and Drug-Induced Liver Injury Detection, *Chem. Commun.*, 2019, **55**, 2541–2544, DOI: 10.1039/C8CC10286D.

43 J. Lu and P. H. Toy, Organocatalytic Decarboxylative Doebner-Knoevenagel Reactions between Arylaldehydes and Monoethyl Malonate Mediated by a Bifunctional Polymeric Catalyst, *Synlett*, 2011, 1723–1726, DOI: 10.1055/s-0030-1260808.

44 E. Nomura, T. Noda, D. Gomi and H. Mori, Substituent Effect on the Formation of Arylindanes by Dimerization of Ferulic Acid and Its Related Compounds, *ACS Omega*, 2018, **3**, 12746–12753, DOI: 10.1021/acsomega.8b01953.

45 B. E. Maryanoff and A. B. Reitz, The Wittig Olefination Reaction and Modifications Involving Phosphoryl-Stabilized Carbanions. Stereochemistry, Mechanism, and Selected Synthetic Aspects, *Chem. Rev.*, 1989, **89**(4), 863–927, DOI: 10.1021/cr00094a007.

46 E. Hernández-Fernández, M. Fernández-Zertuche, O. García-Barradas, O. Muñoz-Muñiz and M. Ordóñez, Practical and Efficient Synthesis of (E)-α,β-Unsaturated Amides Bearing (S)-α-Methylbenzylamine from 2-Phosphonamides via Horner-Wadsworth-Emmons Reaction, *Synlett*, 2006, **47**, 440–444, DOI: 10.1055/s-2006-926265.

47 M. Ordóñez, E. Hernández-Fernández, M. Montiel-Pérez, R. Bautista, P. Bustos, H. Rojas-Cabrera, M. Fernández-Zertuche and O. García-Barradas, A Convenient Method for the Preparation of Chiral Phosphonoacetamides and Their Horner-Wadsworth-Emmons Reaction, *Tetrahedron: Asymmetry*, 2007, **18**, 2427–2436, DOI: 10.1016/j.tetasy.2007.09.033.

© 2024 The Author(s). Published by the Royal Society of Chemistry

Open Access Article. Published on 11 January 2024. Downloaded on 11/12/2024 6:21:54 AM. This article is licensed under a Creative Commons Attribution-NonCommercial 3.0 Unported Licence.

48 H. Ishida, J.-C. Bünzli and A. Beeby, Guidelines for Measurement of Luminescence Spectra and Quantum Yields of Inorganic and Organometallic Compounds in Solution and Solid State (IUPAC Technical Report), *Pure Appl. Chem.*, 2016, **88**, 701–711, DOI: 10.1515/pac-2014-0706.

49 V. Pilla, A. C. Gonçalves, A. A. Dos Santos and C. Lodeiro, Lifetime and Fluorescence Quantum Yield of Two Fluorescein-Amino Acid-Based Compounds in Different Organic Solvents and Gold Colloidal Suspensions, *Chemosensors*, 2018, **6**, 26, DOI: 10.3390/CHEMOSENSORS6030026.

50 L. Xu, S. Zhang, X. Liang, S. Zhong, B. Wang, Z. Li and X. Cui, Novel Biocompatible AIEgen from Natural Resources: Palmatine and Its Bioimaging Application, *Dyes Pigm.*, 2021, **184**, 108860, DOI: 10.1016/J.DYEPIG.2020.108860.

51 X. Zeng, Z. Chen, L. Tang, H. Yang, N. Liu, H. Zhou, Y. Li, J. Wu, Z. Deng, Y. Yu, *et al.*, A Novel Near-Infrared Fluorescent Light-up Probe for Tumor Imaging and Drug-Induced Liver Injury Detection, *Chem. Commun.*, 2019, **55**, 2541–2544, DOI: 10.1039/C8CC10286D.

52 R. Ahmed and A. K. Manna, Understanding High Fluorescence Quantum Yield and Simultaneous Large Stokes Shift in Phenyl Bridged Donor-π-Acceptor Dyads with Varied Bridge Lengths in Polar Solvents, *J. Phys. Chem. A*, 2022, **126**, 4221–4229, DOI: 10.1021/ACS.JPCA.2C02950/SUPPL_FILE/JP2C02950_SI_001.PDF.

53 T. Zhang, Y. Li, J. Yan, Y. Liang, B. Xu, K. Zheng and N. Zhang, Syntheses and Spectroscopic Properties of Substituted Diazaborepins with Large Stokes Shift, *Tetrahedron*, 2018, **74**, 2807–2811, DOI: 10.1016/J.TET.2018.04.063.

54 H. A. Z. Sabek, A. M. M. Alazaly, D. Salah, H. S. Abdel-Samad, M. A. Ismail and A. A. Abdel-Shafi, Photophysical Properties and Fluorosolvatochromism of D–π–A Thiophene Based Derivatives, *RSC Adv.*, 2020, **10**, 43459–43471, DOI: 10.1039/D0RA08433F.

55 M. J. Frisch, G. W. Trucks, H. B. Schlegel, G. E. Scuseria, M. A. Robb, J. R. Cheeseman, G. Scalmani, V. Barone, G. A. Petersson, H. Nakatsuji, X. Li, M. Caricato, A. Marenich, J. Bloino, B. G. Janesko, R. Gomperts, B. Mennucci, H. P. Hratchian, J. V. Ortiz, A. F. Izmaylov, J. L. Sonnenberg, D. Williams-Young, F. Ding, F. Lipparini, F. Egidi, J. Goings, B. Peng, A. Petrone, T. Henderson, D. Ranasinghe, V. G. Zakrzewski, J. Gao, N. Rega, G. Zheng, W. Liang, M. Hada, M. Ehara, K. Toyota, R. Fukuda, J. Hasegawa, M. Ishida, T. Nakajima, Y. Honda, O. Kitao, H. Nakai, T. Vreven, K. Throssell, J. A. Montgomery Jr, J. E. Peralta, F. Ogliaro, M. Bearpark, J. J. Heyd, E. Brothers, K. N. Kudin, V. N. Staroverov, T. Keith, R. Kobayashi, J. Normand, K. Raghavachari, A. Rendell, J. C. Burant, S. S. Iyengar, J. Tomasi, M. Cossi, J. M. Millam, M. Klene, C. Adamo, R. Cammi, J. W. Ochterski, R. L. Martin, K. Morokuma, O. Farkas, J. B. Foresman and D. J. Fox, *Gaussian 09, Revision A.02*, Gaussian, Inc., Wallingford CT, 2016.

56 E. J. Calabrese and R. B. Blain, The Hormesis Database: The Occurrence of Hormetic Dose Responses in the Toxicological Literature, *Regul. Toxicol. Pharmacol.*, 2011, **61**, 73–81, DOI: 10.1016/j.yrtph.2011.06.003.

57 W. H. Van Der Schalie and J. H. Gentile, Ecological Risk Assessment: Implications of Hormesis, *J. Appl. Toxicol.*, 2000, **20**, 131–139, DOI: 10.1002/(sici)1099-1263(200003/04)20:2<131::aid-jat644>3.0.co;2-4.

58 E. J. Calabrese, The Emergence of the Dose-Response Concept in Biology and Medicine, *Int. J. Mol. Sci.*, 2016, **17**, 2034, DOI: 10.3390/ijms17122034.

59 M. P. Mattson, Hormesis Defined, *Ageing Res. Rev.*, 2008, **7**, 1–7, DOI: 10.1016/j.arr.2007.08.007.

60 P. Yang, X. Q. He, L. Peng, A. P. Li, X. R. Wang, J. W. Zhou and Q. Z. Liu, The Role of Oxidative Stress in Hormesis Induced by Sodium Arsenite in Human Embryo Lung Fibroblast (HELF) Cellular Proliferation Model, *J. Toxicol. Environ. Health, Part A*, 2007, **70**, 976–983, DOI: 10.1080/15287390701290832.

61 R. Franco, G. Navarro and E. Martínez-Pinilla, Hormetic and Mitochondria-Related Mechanisms of Antioxidant Action of Phytochemicals, *Antioxidants*, 2019, **8**, 1–12, DOI: 10.3390/antiox8090373.

62 Y. Liu, K. Z. Guyton, M. Gorospe, Q. Xu, J. C. Lee and N. J. Holbrook, Differential Activation of ERK, JNK/SAPK and P38/CSBP/RK Map Kinase Family Members during the Cellular Response to Arsenite, *Free Radical Biol. Med.*, 1996, **21**, 771–781, DOI: 10.1016/0891-5849(96)00176-1.